ARTICLES

Absolute differential cross sections and charge asymmetries for $\pi^{\pm}d$ elastic scattering at 65 MeV

M. D. Kohler, J. T. Brack,* B. Clausen,† J. J. Kraushaar, B. J. Kriss, R. A. Ristinen, and K. Vaziri‡
Nuclear Physics Laboratory, Department of Physics, University of Colorado, Boulder, Colorado 80309

G. R. Smith and D. F. Ottewell
TRIUMF, Vancouver, British Columbia, Canada V6T 2A3

M. E. Sevior and R. P. Trelle
University of British Columbia, Vancouver, British Columbia, Canada V6T 2A3

N. R. Stevenson
University of Saskatchewan, Saskatoon, Saskatchewan, Canada S7N 0W0
(Received 26 December 1990)

Absolute $\pi^{\pm}d$ differential cross sections and charge asymmetries have been measured at an incident pion energy of 65 MeV, using an active target of deuterated scintillator plastic to detect recoil deuterons in coincidence with scattered pions. Statistical and systematic uncertainties in the cross sections are each typically $\pm 3\%$. The charge asymmetry is consistent with theoretical predictions.

I. INTRODUCTION

Interest in $\pi^{\pm}d$ elastic scattering stems from the fact that it is the simplest example of pion scattering from a nucleus and that it can form a basis for understanding pion scattering from more complex nuclei. In principle, the πNN system may be treated exactly with relativistic Faddeev equations [1,2] and hence $\pi^{\pm}d$ data can serve as a test of such calculations. In addition, precise comparison of $\pi^{+}d$ and $\pi^{-}d$ cross sections provides a check on charge symmetry once Coulomb effects have been taken into account. In the present work, we have measured πd elastic differential cross sections at 65 MeV and have compared our results to recent theoretical treatments based on the Faddeev equations [1,2].

There have been few measurements of πd elastic differential cross sections below 100 MeV. In this energy region, two experiments involving only $\pi^{+}d$ cross sections have been reported—one at 82 MeV [3] and another at 47.5 MeV [4]. Neither of these measurements was absolute; they were both normalized to $\pi^{+}p$ cross sections. Balestri *et al.* [5] measured absolute πd cross sections at 65 MeV for both pion polarities. Their experiment employed a liquid-deuterium target and used a range spectrometer to detect the scattered pions. The charge asymmetry data of Balestri *et al.* deviate significantly from the values calculated by Fröhlich *et al.* [1]. This result, and the importance of obtaining precise scattering data in an energy region in which the cross section is sensitive to Coulomb effects and to partial waves other than P_{33}, provided the motivation for the present experiment. Measurements of the energy dependence of the charge asymmetry in πd elastic scattering have been reported by Smith *et al.* [6] for incident pion energies of 143, 180, 220, and 256 MeV.

II. DESCRIPTION OF THE EXPERIMENT

The present experiment was performed at TRIUMF using the M13 beam channel [7]. The pion beam energy was 65.0 ± 0.5 MeV at the center of the target and data were collected for laboratory scattering angles of $70°-140°$ in $10°$ steps. The primary (proton) beam at TRIUMF has a cyclotron time structure with narrow rf pulses spaced by 43 nsec. Thus reliable identification and counting of incident pions with in-beam counters is possible at average beam rates of 10^6 π/sec and an accurate absolute measurement may be performed. The active target was deuterated plastic scintillator [8]. Deuterons which recoiled from an elastic-scattering event were detected in coincidence with the scattered pions using a method described earlier for low-energy $\pi^{\pm}p$ cross-section measurements [9]. A Monte Carlo routine was used to account for pion decay, multiple Coulomb scattering of pions and muons in the scintillators and in the air, and to correct for the loss of scattering events due to the escape of recoil deuterons from the target. The experimental setup is illustrated in Fig. 1, and the placement, dimensions, etc., of the scintillation counters are given in Table I.

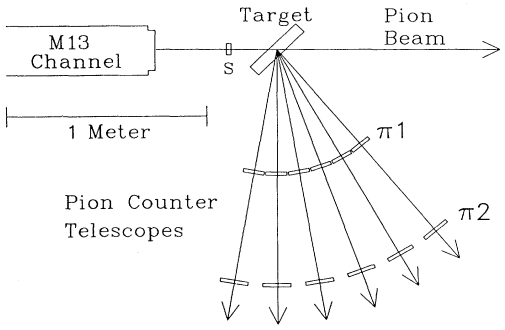

FIG. 1. Counter arrangement for the active target measurement. Data were gathered simultaneously at six scattering angles. All flight paths were in air. Incident particles were identified by rf-referenced TOF to S and by their pulse height in S. Counter dimensions, their distances from the target, etc., are listed in Table I. Note that counters are not drawn to scale, and particles which scattered in S could not be seen by the counter telescopes in the actual setup.

A. Beam monitoring

In order to identify and count beam particles, a beam-defining scintillator (S) was placed upstream of the active target. A beam count was defined as a coincidence between S and the active target. These beam counts were recorded by a scaler. With this arrangement, the accidental coincidence rate in the absence of beam was negligible. Determination of the beam pion fraction was accomplished by collecting time-of-flight and pulse-height information for a sample beam count. The beam was sampled in this way at regular intervals throughout the data-acquisition process. The average sampling rate was about 0.0005% of the beam rate. The pion fraction of the scaled beam for each pion polarity remained constant to within 0.5% throughout the experiment. For the positive-polarity beam tune, the beam at the target was approximately 96% pions. For the negative-polarity tune, the beam at the target was approximately 91% pions. The remaining particles were muons and electrons. In addition, some beam bursts contained more than one pion. The methods used to account for muons, electrons, and beam multiples, and to remove protons from the beam, are discussed below.

The 65-MeV π^+ tune in the M13 channel at TRIUMF consists predominantly of protons before it reaches a CH_2 degrader placed between the first and second bending magnets. The thickness of the degrader was chosen so that protons which pass through the first bending magnet lose half of their energy as they pass through the degrader. These protons are then separated from the pions by the second bending magnet. Any protons remaining in the beam leave a signal in S several times larger than that produced by a passing pion. These protons were removed by an upper-level hardware pulse-height cutoff applied to this scintillator and therefore did not contribute to beam counts. Moreover, these protons did not have sufficient energy to pass through the S scintillator and therefore could not reach the target.

Muons and electrons were accounted for by determining their fractions in the beam and adjusting the number of beam counts accordingly. The beam fractions of muons and electrons which originated at the production target were determined using the time-of-flight (TOF) data collected for the sample beam counts. The TOF of beam particles was measured relative to the rf pulses which accelerate each beam burst of the primary proton beam. A typical TOF spectrum with peaks corresponding to pions, muons, and electrons is shown in Fig. 2. Muons and electrons which originated at the production target made up about 2% of the of the π^+ beam and 7% of the π^- beam at the target. An additional 2% of the beam consisted of muons which came from pion decay after the last channel bending magnet. These muons could not be distinguished from pions by TOF. The fraction of these muons in the beam was determined using the Monte Carlo simulations. The simulations are discussed in detail in Sec. II D.

During the experiment, the rate of pions incident on the target varied from 0.4×10^6 to 3.1×10^6 π/sec. This corresponds to a range of less than 1% to about 7% for the probability that a single rf pulse will contain more than one pion. However, the beam as defined by a coin-

TABLE I. Scintillation counters illustrated in Fig. 1.

Counter	S	T	$\pi1$	$\pi2$
Material	CH, BC412[a]	CD, NE125[b]	CH, BC412[a]	CH, BC412[a]
Purpose	beam definition	target, recoil d detection	scattered π detection	scattered π detection, solid angle definition
Distance from target (cm)	26.0	0.0	66.0	123.7
Dimensions (cm) (horiz.×vert×thick)	2.0×3.0×0.16	8.86×5.02×0.18	9.0×20.0×0.32	2.0×30.0×0.32
In event trigger	yes	yes	yes	yes
In beam trigger	yes	yes	no	no

[a]Bicron Corporation, Newbury, OH.
[b]Nuclear enterprises, Ltd., Fairfield, NJ.

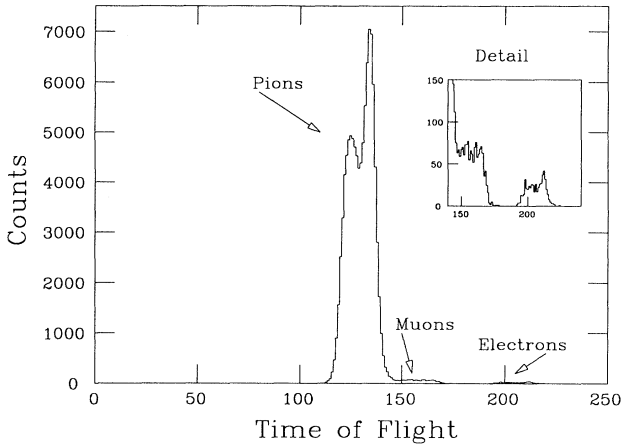

FIG. 2. rf-referenced TOF spectrum of 65-MeV π^+ beam incident on counter S. The TOF is given in arbitrary units. The beam was sampled at regular intervals and time-of-flight information was recorded so that the fraction of pions in the beam could be determined. The double peaking is due to the time structure of the primary proton beam produced by the TRIUMF cyclotron.

cidence of the S scintillator and the target has a different multiples fraction than the beam on the target. This is a consequence of the fact that the rate of pions incident on S was only about half as large as the rate incident on the target. The presence of S in the beam definition removed about half of the single pions incident on the target, but only about one-quarter of the doubles. Thus the beam defined by our experimental setup had a range of about 1% to about 11% for the probability that a single rf pulse which produced a coincidence of S and the target contained more than one pion. In order to calculate the number of pions incident on the target which passed our beam definition, the number of observed coincidences was multiplied by a factor f_m. This factor was calculated as follows:

$$f_m = \frac{P_1 + 2P_2 + 3P_3 + \cdots}{P_1 + P_2 + P_3 + \cdots} ,$$

where P_n is the probability (calculated using Poisson statistics) that a single rf pulse will contain n pions and the P_n's are corrected for the effect of the beam-defining scintillator. Cross section data for $\pi^+ d$ scattering at 95.9° (c.m.) were collected for a range of beam rates corresponding to a range of 1.02–1.11 for f_m. No dependence of the measured cross sections on the beam rate was observed (see Fig. 3).

The above discussion translates into a calculation which converts the raw beam counts (the number of coincidences between S and the active target), B_{raw}, to the number of pions used to calculate the cross section:

$$B = B_{\text{raw}} f_\pi f_m ,$$

where f_π is the pion fraction and f_m is the multiples factor. In Table II the values of B_{raw}, f_π, f_m, and other

TABLE II. Terms used to calculate $(d\sigma/d\Omega)_{\pi^+}^{\text{c.m.}}$ for $\theta_\pi^{\text{c.m.}} = 95.9°$ from one (of three) sets are listed with their percent uncertainties. An uncertainty of 0.5 MeV in the beam energy was not taken into account in the error analysis. See Sec. III for discussion of each term. All uncertainties listed represent one standard deviation.

Term	Value	% Uncertainty
	statistical and random errors	
Yield	7272	3.6
$(1-f_{\text{esc}})$	0.98	0.4
$d\Omega_{\text{eff}}^{\text{c.m.}}$	16.8 msr	1.9[a]
$\theta_\pi^{\text{c.m.}}$	95.9°	0.5°, 0.6%[b]
$(1-r_d)$	0.996	0.2
$(1-r_\pi)$	0.99	0.5
	overall statistical and random error = 4.2%	
	normalization errors	
B_{raw} (beam)	6.44×10^{10}	
f_π (pion fraction)	0.96	0.5
f_m (multiples factor)	1.1	0.5
f_l (live time)	0.82	0.5
$\cos\theta_T$	0.707	0.4
T (target thickness)	8.4×10^{21} deuterons/cm^2	2.4
	overall normalization error = 2.6%	

[a]This includes a 1.0% statistical uncertainty in the Monte Carlo simulation as well as 1.6% uncertainty in the measurement of the geometric solid angle subtended by the $\pi 2$ counter.
[b]For $\theta_\pi^{\text{c.m.}}$, the first number is the absolute error and the second number is the resulting percent uncertainty in the cross sections.

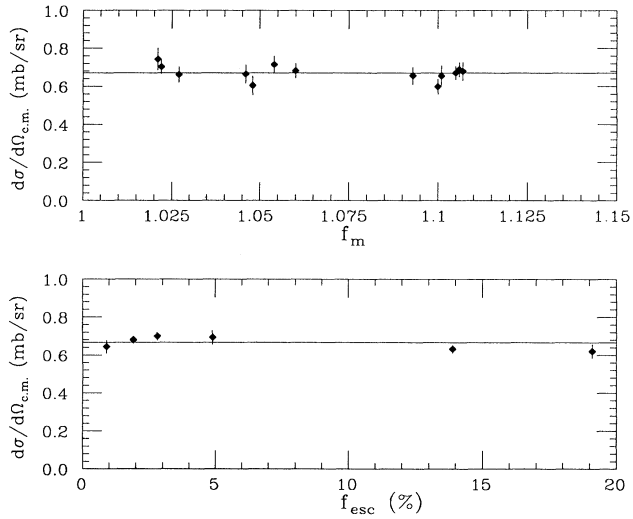

FIG. 3. Dependence of the measured cross section on beam rate and target angle. The top plot shows $\pi^+ d(\theta_\pi^{\text{c.m.}} = 95.9°)$ cross-section data collected at beam rates on target ranging from 0.6 to 3.1 MHz with the corresponding correction for multiple pions ranging from about 2% to 11%. The bottom plot shows $\pi^+ d$ $(\theta_\pi^{\text{c.m.}} = 95.9°)$ cross-section data collected with six different target angles with the corresponding escape fraction ranging from about 1% to 19%. The measured cross sections are not dependent on beam rate or target angle.

quantities which are described below are listed along with their uncertainties for one data set.

B. Pion counters

Scattered pions were detected in six pion counter telescopes, each of which consisted of two plastic scintillators (see Fig. 1). This setup allowed us to collect cross-section data at six different angles simultaneously. The counter telescopes were placed with their centers 10° apart and each subtended a solid angle of 17.5 msr as seen from the target. Each $\pi 1$ counter was viewed by a single photomultiplier. Two photomultipliers were used for the $\pi 2$ counters, one attached above and one below the scintillator. The signals collected by the two $\pi 2$ photomultipliers were summed for amplitude analysis, and the mean time was used to achieve good time resolution. A resolution of 400 psec full width at half maximum was obtained for the TOF of particles between the S scintillator and the $\pi 2$ counter. In order for a scattering event to be written to tape, a coincidence was required of $\pi 1$, $\pi 2$, S, and the active target where $\pi 1$ and $\pi 2$ must belong to the same counter telescope. The efficiency of these counters and associated electronics has been checked in a separate set of tests and was found to be in the range of 0.995–1.000 over an energy range of 20–100 MeV for both positive and negative pions [9,10]. In the analysis the counter efficiency was taken to be 1.000 and an uncertainty of 0.5% was added in quadrature to the statistical uncertainty in the yield.

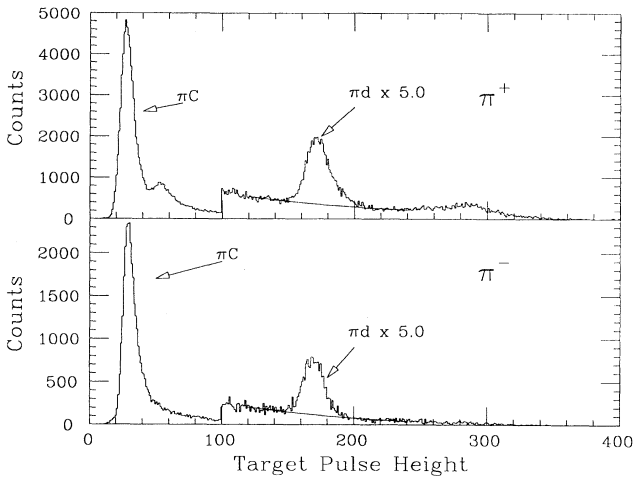

FIG. 4. Target pulse-height spectra for $\pi^+ d$ and $\pi^- d$ elastic scattering at $\theta_\pi^{\text{c.m.}} = 95.9°$. The target pulse height is given in arbitrary units. The peak due to elastic and inelastic scattering from carbon is well separated from the πd recoil deuteron peak. In the π^+ spectrum, the background under the πd peak is mostly due to deuteron breakup, pion absorption, and pion-nucleon quasielastic scattering. In the π^- spectrum, the background is smaller since the absorption events are absent and the quasielastic $\pi^- p$ cross section is relatively small. Also shown are second-degree polynomial least-squares fits to the background. The fitted background was subtracted from the peak in order to obtain the yield.

C. Active target

The target in this experiment was an NE125 deuterated plastic scintillator [8]. It had a $^2H/^1H$ ratio of 26:1 and a $(^2H+^1H)/C$ ratio of 0.996 specified by the manufacturer. A commercial laboratory [11] provided both mass spectrometric and infrared absorption determinations of the deuteron-to-proton ratio as well as elemental microanalysis of the carbon–to–total-hydrogen ratio. The carbon–to–total-hydrogen ratio differed from the manufacturer's specification by 1%, and the deuteron-to-proton ratio was 1% higher than specified, leading to a deuteron density 1% higher than that given by the manufacturer. This higher number is incorporated into the number of deuterons per square centimeter used in the calculation of the cross sections.

The active target was used to detect the recoil deuteron from an elastic-scattering event. It was viewed by two photomultipliers, and the target pulse height was recorded for each scattering event. Figure 4 shows target pulse-height spectra for π^+ and π^- scattering at $\theta_\pi^{\text{c.m.}} = 95.9°$. The peaks corresponding to elastic and inelastic pion-carbon scattering and elastic pion-deuteron scattering are labeled in the figures. The separation of the peaks is largely a result of the characteristic response of plastic scintillators to different recoil particles. A deuteron which stops in the active target will produce a light output about 10 times greater than a carbon nucleus with similar energy [12]. In this experiment the recoil carbon nuclei produced in πC scattering events had substantially less energy than the recoil deuterons. As a result, for a given pion-scattering angle, the light output from recoil carbon nuclei was about 100 times smaller than that produced by the recoil deuterons. In fact, the pulse height of the carbon peak in Fig. 4 is due almost entirely to the passage of the pion through the target. The pulse height of the deuteron peak is a sum of the light output of the incident and scattered pion and the recoil deuteron. The broad peak to the right of the deuteron peak in the π^+ spectrum (Fig. 4, top) arises from

TABLE III. Center-of-mass $\pi^+ d$ and $\pi^- d$ cross sections and asymmetries at $T_\pi = 65.0$ MeV and their random uncertainties. An additional normalization uncertainty of ±2.6% applies to the cross-section data. The systematic uncertainty in the asymmetry is ±1.0% and is not included in the errors shown.

$\theta_\pi^{\text{c.m.}}$ (deg)	$(d\sigma/d\Omega)_{\pi^+}^{\text{c.m.}}$ (mb/sr)	$(d\sigma/d\Omega)_{\pi^-}^{\text{c.m.}}$ (mb/sr)	Asymmetry (%)
75.6	0.566±0.020	0.635±0.031	5.7±2.7
85.9	0.567±0.019	0.608±0.027	3.5±2.4
95.9	0.681±0.016	0.674±0.021	−0.3±1.5
105.8	0.772±0.020	0.739±0.034	−1.5±1.9
115.5	0.898±0.025	0.890±0.036	−0.2±1.5
125.1	1.009±0.025	1.077±0.034	3.5±1.4
134.5	1.114±0.037	1.180±0.035	2.8±1.6
143.7	1.259±0.050	1.310±0.050	2.0±1.5

$^{12}C(\pi^+,\pi^+p)$ quasifree scattering. This peak is not evident in the π^- spectrum (Fig. 4, bottom) because the π^-p cross section is about 6 times smaller than the π^+p cross section at 65 MeV for a center-of-mass scattering angle of 95.9°. The shoulder on the carbon peak in the π^+ spectrum is due to the passage of two pions through the target ($P_2/P_1=10\%$ for the π^+ spectrum). This feature does not appear in the π^- spectrum because it was taken with a much lower beam rate ($P_2/P_1=1\%$ for the π^- spectrum). The large difference in the beam rates occurs because the M13 channel tune was not changed when the beam polarity was reversed so that the calculation of the charge asymmetry would not be compromised. In both spectra there is a smooth background due to scattering events in which the deuteron broke up into a neutron and a proton. For π^+d scattering absorption processes also contribute to the smooth background. The breakup background arises from two sources: the deuteron can break up directly in an inelastic-scattering event or an elastically scattered deuteron can break up due to interactions in the target. The latter effect causes a loss of elastic events and must be corrected for in the analysis (see Sec. III). More detail about the active target method can be found in Ref. [9].

D. Monte Carlo simulations

The GEANT [13] Monte Carlo code was used to account for effects due to the escape of recoil deuterons from the target, in-flight decay of pions and multiple Coulomb scattering of pions and muons in the scintillators and air. The statistical uncertainties in the Monte Carlo simulations add about 1% to the uncertainties in the cross sections.

During the experiment, six different target angles were used with three different sets of angles for the pion telescopes. There were a total of six different geometries (i.e., combinations of target angle and angle sets) to be simulated by the Monte Carlo routine. More than 80% of the data were collected using three near-optimum geometries, and the results listed in Table III (and illustrated in Figs. 7–9) were obtained using these data. The data from the other three setups were used to confirm that the results are independent of geometry. In each simulation the Monte Carlo routine generated approximately 2×10^6 pions. The pions began their simulated flight at a point 56 cm upstream of the target. In order to approximate the actual beam as closely as possible, the initial pions were generated at random points in the plane perpendicular to the beam axis according to a Gaussian distribution representative of the known beam spot size at the target. However, reducing the beam spot size to zero produced no discernible change in the results of the simulations. The momentum of each pion was randomly chosen by the program according to a Gaussian distribution about the central momentum corresponding a 1% spread in the longitudinal component of momentum. When a pion reached the downstream surface of the target, its flight was stopped by the program and a point along its path in the target was chosen at random to be the πd vertex. A scattered pion trajectory was then chosen at random within a user-defined solid angle ($d\Omega_{MC}$), which was large enough to ensure that a pion on the edge of this solid angle could not cause any of the counter telescopes to fire even if the pion were to decay. Pions were tracked until they or their decay muons passed through or beyond the counter telescopes. Approximately 10 000 simulated events were accumulated in each counter telescope for each geometry.

In order to minimize the number of recoil deuterons which escape from the target, the target angle was set so that recoil deuterons would have trajectories parallel to the target surface. However, since data were collected for six scattering angles simultaneously, this could not be strictly true for all six angles. The number of events lost depended on the target angle and on the pion-scattering angle. The fraction of lost events was determined by calculating the ratio f_{esc} of "escapes" to total events obtained in the Monte Carlo simulations. An escape is a simulation event in which the pion passes through S, the target, and a counter telescope, while the recoil deuteron escapes from the target. We assumed that all of the simulation events in which the deuteron escaped from the target corresponded to events that were lost in the actual experiment. However, the simulations revealed (not surprisingly) that up to 20% of the escaping deuterons leave enough energy in the target to fall under the deuteron peak in the target pulse-height spectrum. The remaining escape deuterons fall to the left of the peak and contribute to the background in this region. The subtraction of the fitted background from the peak removes the escape deuterons which fall under the peak. However, an uncertainty of 20% (in addition to the statistical uncertainty) in the quantity f_{esc} was assumed since the shape of the background produced by the escaping deuterons is not well understood. The total number of observed events was divided by the quantity $(1-f_{esc})$ in order to obtain the true number of events. Cross sections were measured using six different target angles, and f_{esc} varied from 1% to 19%. No dependence of the measured cross sections on the target angle was observed (see Fig. 3).

As mentioned in Sec. II A, pion decay after the channel exit and upstream of the target can cause spurious beam counts. The beam counts in the Monte Carlo simulation consisted of three types: pions which hit S and the target, muons which hit S and the target, and pions which hit S and then decayed into muons which hit the target. The two types of counts in which the particle at the target is a muon contribute 0.2% and 1.8%, respectively, to the total. Thus, when calculating the cross sections, the scaled beam counts were reduced by approximately 2% to account for pion decay.

Decay and Coulomb scattering of scattered pions caused a net loss of event counts. About 16% of the scattered pions whose initial trajectories passed through a counter telescope decayed into muons before they could be detected. About $\frac{3}{4}$ of these muons did not pass through the counter telescope. So a scattered pion whose trajectory passed through a telescope was not detected about 12% of the time, thus causing an event to be lost. Some scattered pions whose trajectories did not pass

through a telescope decayed into muons which did pass through a telescope, thus creating a spurious event. These competing effects caused a net event loss of about 5%. Changes in pion and muon trajectories due to multiple Coulomb scattering were also considered in the simulations. The effects of multiple Coulomb scattering on our Monte Carlo simulations were smaller than the statistical errors.

Effects due to decay and Coulomb scattering of scattered pions were incorporated into the cross-section calculation via a solid-angle correction to each of the individual counter telescopes. The effective solid angle of a telescope is given by

$$d\Omega_{\text{eff}}^{\text{lab}} = \frac{n}{N} d\Omega_{\text{MC}}^{\text{lab}} ,$$

where n is the number of simulated events counted in the telescope, N is the total number of scattered pions generated in the simulation, and $d\Omega_{\text{MC}}$ is the solid angle into which the Monte Carlo routine allowed the pions to scatter. The Monte Carlo solid angle generously enclosed the array of counter telescopes so that increasing the size of $d\Omega_{\text{MC}}$ did not change the calculated effective solid angle. When the routine was instructed to ignore pion decay and multiple Coulomb scattering, the effective solid angles which it calculated were equal to the geometric solid angles subtended by the counter telescopes within the statistical uncertainty of the simulation. Further details regarding the use of the Monte Carlo routine can be found in Ref. [9].

III. DATA ANALYSIS

Differential cross sections were calculated as follows:

$$\frac{d\sigma(\theta_\pi)}{d\Omega^{\text{c.m.}}} = \frac{Y \cos\theta_T}{(1-f_{\text{esc}})(1-r_d)(1-r_\pi)B(d\Omega_{\text{eff}}^{\text{c.m.}})Tf_1} ,$$

where Y (yield) is the total number of observed elastic πd events for pion-scattering angle θ_π, f_{esc} is the recoil deuteron escape fraction, r_d is the fraction of elastic πd events lost due to deuteron-nuclear interactions in the CD target, r_π is the fraction of elastic πd events lost due to pion-nuclear interactions in the target, air, and scintillators, θ_T is the angle between the beam and normal to the target, B is the number of pions incident on the target, $d\Omega_{\text{eff}}^{\text{c.m.}}$ is the effective solid angle subtended by the pion counter telescope as calculated by the Monte Carlo program, T is the number of deuterons per unit area in the target, and f_1 is the computer live time fraction.

In order to determine the yield, it was necessary to separate various contaminant reactions from the πd reac-

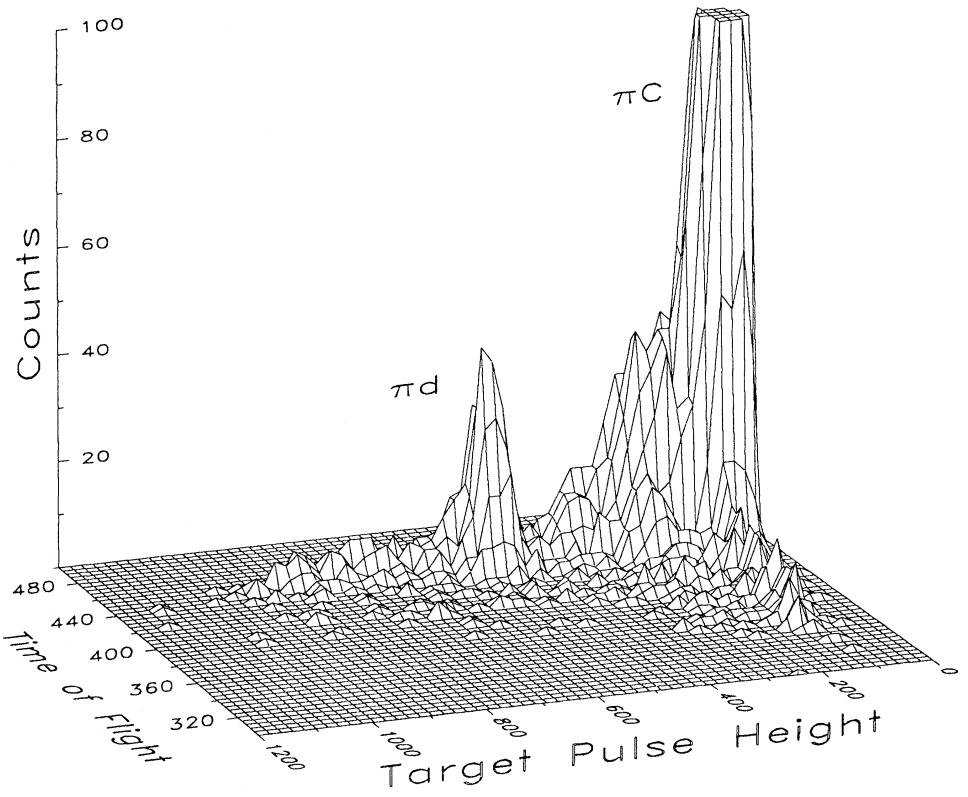

FIG. 5. Three-dimensional plot of pion TOF between the S scintillator and the $\pi 2$ scintillator versus target pulse height. Both the TOF and pulse height are given in arbitrary units. Events plotted are for π^+ scattering with $\theta_\pi^{\text{c.m.}} = 95.9°$. Events with a TOF larger than 460 were removed from the analysis and do not appear here. The majority of these removed events were caused by protons from π^+ absorption processes. The πC peak is truncated at 100 counts.

tions. The most important contaminant reactions were pion elastic scattering from carbon, pion absorption on deuterons and quasideuterons in the carbon nuclei, pion scattering from quasifree protons in the carbon nuclei, and deuteron breakup. A three-dimensional plot of target pulse height vs TOF to the $\pi 2$ counter for π^+ scattering (Fig. 5) shows these reactions and the extent to which they are separated. The events between the peaks in Fig. 5 are due to absorption and breakup processes. The breakup and absorption events leave a continuum of energies in the target. Many of these events were removed using a cut on the TOF between the S scintillator and $\pi 2$ counter. The measured cross section does not depend on the position of this cut as long as it is made far enough away from the πd events. Those events that remained constituted a smooth background in the one-dimensional target pulse-height spectra (Fig. 4). This background was fit by a second-degree polynomial and subtracted from the deuteron peak to obtain the yield. Typical fits are shown in Fig. 4. With one exception, all fits used gave a χ^2/ν between 0.5 and 1.5. Figure 6 is a superposition of pulse-height spectra for pion-scattering angles between 70° and 140° in the laboratory. This figure illustrates the smoothness of the background throughout the range in which the fits were performed.

The correction to the yield for deuteron-nuclear reactions in the target includes a contribution from $d \rightarrow np$ breakup of elastically scattered deuterons as well as other nuclear reactions. The correction for breakup reactions was based on a cross section of 300 mb for 18-MeV deuterons inferred from the work Peterson *et al.* [14]. The size of this correction ranged from 0.02% for the smaller pion-scattering angles to 0.3% for the larger angles. The correction for deuteron-nuclear reactions other than breakup was scaled from the work of Measday and Richard-Serre [15] for proton-nuclear reactions and ranged from 0.1% to 0.3%.

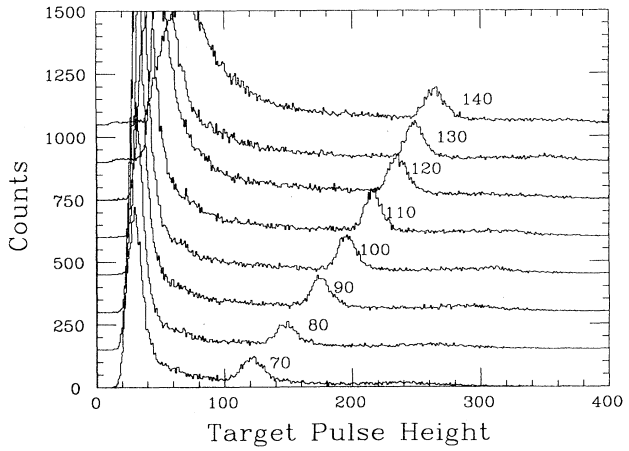

FIG. 6. Target pulse-height spectra for laboratory $\pi^+ d$ scattering angles from 70° to 140°. The target pulse height is given in arbitrary units. This figure illustrates the smoothness of the background in the region in which the fits were performed. For clarity, the base lines are shifted up by 150 counts for each 10° increase in pion scattering angle.

The correction to the yield for pion-nuclear reactions (r_π) was estimated to be (1.0±0.5)%. This estimate is based on known total pion-nuclear reaction cross sections [16].

The Monte Carlo calculation of the effective solid angle and escape fraction is discussed in Sec. II D. The determination of B is discussed in Sec. II A. The determination of T is discussed in Sec. II C.

IV. ERROR ANALYSIS

Average statistical uncertainties were 3.0% for $\pi^+ d$ cross sections and 3.8% for $\pi^- d$ cross sections. The contributions from various factors to the uncertainties are listed in Table II for one data set. The largest contribution to the statistical errors came from counting statistics and background fitting statistics. Counting statistics result from fluctuations in the region of the πd peak in Fig. 4. Fitting statistics result from fluctuations in the regions to the left and right of the peak, which were used to assess the background. These fluctuations are manifested in the uncertainties in the coefficients calculated by the least-squares fitting routine. The statistical uncertainties in the Monte Carlo simulations also made a significant contribution to the errors. These uncertainties were calculated from the number of simulation events collected and also from the standard deviation of the distribution of results obtained form repeated simulations. The two methods of calculating the Monte Carlo uncertainties gave consistent results.

The overall normalization uncertainty in the $\pi^+ d$ and $\pi^- d$ cross sections was 2.6%. The largest normalization uncertainty (2.4%) came from the determination of the number of deuterons per square centimeter in the target. The separation of pions and muons using TOF could not be perfect since muons overlapped with pions in the TOF spectrum (see Fig. 2). The uncertainty in the pion fraction due to this overlap was estimated to be 0.5% (the muon fraction is about 1%). Estimates of these and other normalization uncertainties are listed in Table II. An additional uncertainty due to imperfect knowledge of the beam energy (65.0±0.5 MeV) is not included in the stated normalization uncertainty.

V. RESULTS AND DISCUSSION

The $\pi d \rightarrow \pi d$ reaction yields immediate information concerning isospin conservation. Strict conservation of isospin requires that $\pi^- d$ and $\pi^+ d$ elastic differential cross sections be equal. In practice, the cross sections differ because of Coulomb effects and the inequality of the quark masses. The difference in cross sections is parametrized as the charge asymmetry,

$$A_\pi = \frac{(d\sigma/d\Omega)_{\pi^-} - (d\sigma/d\Omega)_{\pi^+}}{(d\sigma/d\Omega)_{\pi^-} + (d\sigma/d\Omega)_{\pi^+}} .$$

The random errors in A_π listed in Table III were calculated from the uncertainties in the yield and pion-scattering angle. The uncertainties in the other quantities listed in the first part of Table II cancel in the calculation of A_π. The uncertainty in the target deuteron density

also cancels. As a result the normalization error in A_π is approximately 1.0%.

The theoretical calculation of A_π is very sensitive to the treatment of the Coulomb part of the interaction. This is quite difficult to handle in a Faddeev calculation. In Ref. [1] approximations for Coulomb effects were used in order to make the calculation more tractable. Errors on values of A_π obtained in the present work are 1%–3% or about the same size as the value of A_π itself. Because of the uncertainties in both experiment and theory, a difference between the two would be discernible only if it exceeded about 2%.

The differential cross sections and charge asymmetry A_π from this experiment are shown in Figs. 7–9, and the numerical results are listed in Table III. Also shown in Figs. 7–9 are the results of Balestri *et al.* [5] and calculations of Fröhlich *et al.* [1], Garcilazo [2] (Figs. 7 and 8), and Rockmore and Saghai [17] (Fig. 9).

For the $\pi^+ d$ differential cross sections, the agreement of the present data with Balestri *et al.* is quite good except around 135°. The agreement with the $\pi^- d$ data (see Fig. 8) is less encouraging. The comparison of the two sets of data for A_π is shown in Fig. 9 and here some discrepancies are apparent. The most striking differences are the large values of A_π obtained by Balestri *et al.* in the 95°–115° angular range. There is no evidence for such a bump in the present data.

The Faddeev calculations of Fröhlich *et al.* [1] used five different prescriptions for the Coulomb effects and included real pion absorption. The solid and dashed curves in Figs. 7 and 8 are the extremes of the five different Coulomb treatments considered by Fröhlich *et al.* The treatment (a) is the simplest and (e) the most complete.

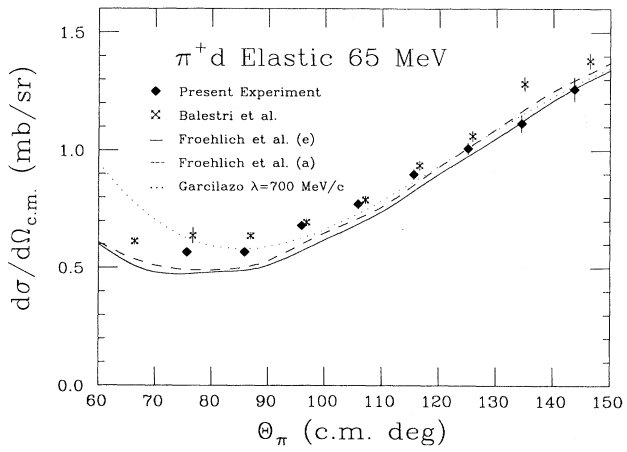

FIG. 7. Center-of-mass cross sections for $\pi^+ d$ elastic scattering at 65.0 MeV from the present experiment, from Balestri *et al.* [5] and from calculations by Fröhlich *et al* [1] and Garcilazo [2]. The two theoretical curves due to Fröhlich *et al.* correspond to (a) the simplest treatment of Coulomb effects and (e) the most comprehensive considered. The calculations of Garcilazo are shown for $\lambda = 700$ MeV/c; they do not distinguish between $\pi^+ d$ and $\pi^- d$ scattering. The error bars shown for the present experiment do not include normalization errors.

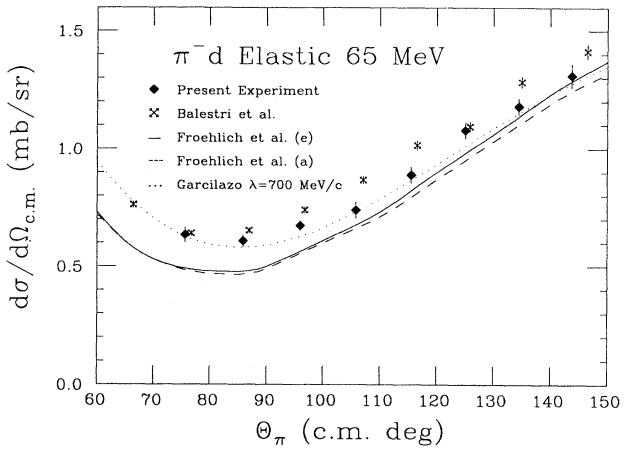

FIG. 8. Same as Fig. 7, but for $\pi^- d$ scattering.

The effect of the different Coulomb treatments on either the $\pi^- d$ or $\pi^+ d$ differential cross sections is not very pronounced. The calculated cross sections tend to lie significantly below the measured values for the smaller scattering angles where the effects of Coulomb-nuclear interference are most pronounced.

Garcilazo [2] has also completed relativistic Faddeev calculations for πd elastic scattering. These calculations do not distinguish between $\pi^+ d$ and $\pi^- d$ scattering. In Garcilazo's model there is only one free parameter λ, which is the cutoff of the πN monopole form factor. Values of λ of 1000, 700, and 500 MeV/c were compared with the data shown in Figs. 7 and 8, and only $\lambda = 700$ MeV/c provided a reasonable description of the data.

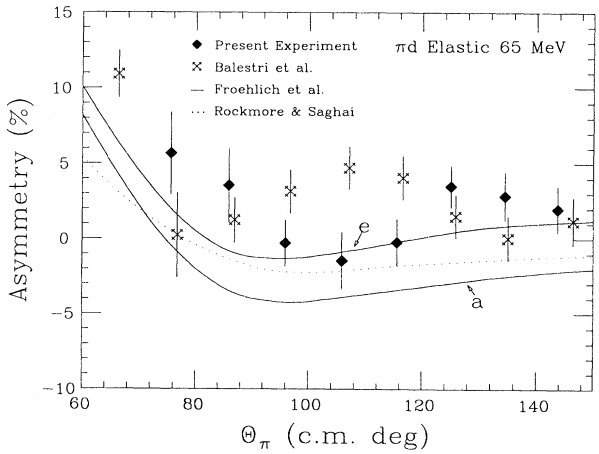

FIG. 9. Charge asymmetries for πd elastic scattering at 65.0 MeV including data from the present experiment, the work of Balestri *et al.* [5], and calculations of Fröhlich *et al.* [1] and Rockmore and Saghai [17]. The bump in the asymmetry reported by Balestri *et al.* in the angular range of 95°–115° was not reproduced by the present experiment. The two theoretical curves of Fröhlich *et al.* shown in the figure correspond to (a) the simplest treatment of Coulomb effects and (e) the most comprehensive. The error bars shown for the present experiment are as listed in Table III.

The results of Fröhlich *et al.* [1] for the charge asymmetry are shown in Fig. 9. These calculations do not include any charge-symmetry-breaking mechanisms for the hadronic forces such as the mass differences of the Δ isobars. In Fig. 9 the treatment (e) provides a better description of the present data than does the simpler Coulomb treatment (a).

Rockmore and Saghai have used the impulse approximation to calculate the charge asymmetry for $T_\pi \leq 100$ MeV and have included the effects of Coulomb distortion, the Δ-isobar mass differences, and internal Coulomb corrections. They predict the charge asymmetry at 65 MeV in order to make comparison with the data of Balestri *et al.* with corrections for the above effects included one at a time in their calculations. None of their predictions produced a bump in the 95°–115° angular region. The closest description of the present data provided by their calculations is shown in Fig. 9, where the calculations shown by the dotted line were carried out without Coulomb distortion effects, Δ-mass perturbation, or spectator mass-difference perturbations.

In summary, we have measured $\pi^{\pm}d$ elastic differential cross sections and charge asymmetries at an incident pion energy of 65 MeV using an active target technique. As expected, discrepancies between theory and experiment are largest for scattering angles for which Coulomb effects are important. The present study has not reproduced the bump in the charge asymmetry parameter in the 95°–115° angular range found in a previous work [5].

ACKNOWLEDGMENTS

We thank H.Garcilazo for providing cross-section calculations and the technical and support staff of TRIUMF for their assistance. This work was supported in part by the U.S. Department of Energy and the Natural Sciences and Engineering Research Council of Canada.

---

*Now at TRIUMF, Vancouver, British Columbia, Canada V6T 2A3.
†Now at Loma Linda University, Loma Linda, CA 92350.
‡Now at Rensselaer Polytechnic Institute, Troy, NY 12181.

[1] J. Fröhlich, B. Saghai, C. Fayard, and G. H. Lamot, Nucl. Phys. **A435**, 738 (1985).
[2] H. Garcilazo, Phys. Rev. C **35**, 1804 (187); (private communication).
[3] K. Gabathuler *et al.*, Nucl. Phys. **A350**, 253 (1980).
[4] D. Axen, G. Duesdieker, L. Felawka, Q. Ingram, R. Johnson, G. Jones, D. Lepatourel, M. Salomon, W. Westlund, and L. Robertson, Nucl. Phys. **A256**, 387 (1976).
[5] B. Balestri *et al.*, Nucl. Phys. **A392**, 217 (1983).
[6] G. R. Smith *et al.*, Phys. Rev. C **38**, 240 (1988).
[7] C. J. Oram, J. B. Warren, G. M. Marshall, and J. Doornbos, Nucl. Instrum. Methods **151**, 445 (1978).
[8] Nuclear Enterprises Ltd. Fairfield, NJ.
[9] J. T. Brack *et al.*, Phys. Rev. C **41**, 2202 (1990).
[10] J. T. Brack *et al.*, Phys. Rev. C **34**, 1771 (1986).
[11] TEO Research Ltd., Vancouver, BC V5W 1E7, Canada.
[12] F. D. Becchetti, C. E. Thorn, and M. J. Levine, Nucl. Instrum. Methods **138**, 93 (1976).
[13] GEANT version 3.10, Data Handling Division, Report No. CERN DD/EE/84-1, 1984.
[14] R. J. Peterson, C. A. Fields, R. S. Raymond, J. R. Thieke, and J. L. Ullman, Nucl. Phys. **A408**, 221 (1983).
[15] D. F. Measday and C. Richard-Serre, CERN Yellow Report No. 69-17, 1969.
[16] A. S. Carrol, I-H. Chiang, C. B. Dover, T. F. Kycia, K. K. Li, P. O. Mazur, D. N. Michael, P. M. Mockett, D. C. Rahm, and R. Rubinstein, Phys. Rev. C **14**, 635 (1976).
[17] R. Rockmore and B. Saghai, Phys. Rev. C **28**, 2064 (1983).